opment (5–7), suggesting a possible interaction between *SF1* and *CXorf6*.

Mastermind-like 2 (MAML2; alias, Mam-3) is a non-DNA-binding transcriptional co-activator in Notch signaling (8, 9) that plays an important role in cell differentiation in multiple tissues by exerting either inductive or inhibiting effects according to the context of the cells (10). Upon ligand-receptor interaction, Notch intracellular domain (N-ICD) is translocated from the cell surface to the nucleus and interacts with a DNA-binding transcription factor, recombination signal binding protein-J (RBP-J), to activate target genes like hairy/enhancer of split 1 (*Hes1*) and *Hes5* (11). In this canonical Notch signaling process, MAML2 forms a ternary complex with N-ICD and RBP-J at nuclear bodies, enhancing the transcription of the Notch target genes (8, 9, 12–14).

However, not all *Hes* genes are activated by the canonical Notch signaling pathway (11, 15, 16). Among such a distinct class of *Hes* genes, recent studies have shown that *Hes3* can be induced by stimulation with a Notch ligand, via a STAT3 (signal transducer and activator of transcription 3)-mediated pathway (17). This finding, together with the lack of *Hes3* induction by N-ICD (16), implies that *Hes3* represents a target gene of a noncanonical Notch signaling.

Here, we report that *CXorf6* produces a protein that has a structural homology with MAML2 and transactivates the *Hes3* promoter activity and that *CXorf6* is involved in testosterone production and harbors an *SF1* target sequence.

EXPERIMENTAL PROCEDURES

Structural Analysis of CXorf6 Protein—We searched BLAST and TBlastn data bases using the CXorf6 protein sequence (NP_005482) as a bait. Protein sequences for the CXorf6 orthologs were predicted by comparing the human CXorf6 sequence with the genomic and transcribed sequences of different organisms using Clustal_X (18). The unrooted phylogram was generated by Clustal_X (18) from the sequence alignment of CXorf6 proteins and was visualized using TreeView 1.6.6 (19).

Primers, Probes, and Small Interfering RNAs (siRNAs)—The sequences of primers, probes, and siRNAs utilized in this study are summarized in supplemental Table 1.

Plasmid Vectors Utilized for CXorf6 Analyses—The cDNAs of the full-length *CXorf6* (amino acids 1–701) and the minor splicing variant lacking exon 4 (ΔExon 4) were amplified from human fetal testis cDNA (Invitrogen) and subcloned into pEF-BOS vector (20) to construct the CXorf6 expression vector for the transactivation analysis. The expression vectors containing cDNAs of nonsense mutants and missense variants of *CXorf6* were constructed by mutagenesis. For the subcellular localization analysis, cDNAs for the wild-type, mutant, and variant *CXorf6* were designed to lose the start codon and fused to the C-terminal side of the gene encoding either red fluorescent protein (RFP) in pDsRED-monomer C1 vector or green fluorescent protein (GFP) in pAcGFP1-C1 vector (Clontech). For the Western blot analysis, cDNAs missing the start codon were subcloned into pCMV-Myc vector (Clontech).

We also utilized the following vectors reported in the literature: pEF-BOSneo-mNotch1 RAMIC with cDNA of mouse *N1-ICD* (21), pEF-BOSneo-aNotch2 with cDNA of mouse *N2-ICD* (22), pEF-BOS-Mam3 with cDNA of human *MAML2* (8), pHes1-luc with the promoter sequence of mouse *Hes1* (−467 ~ +46 bp), pHes5-luc with the promoter sequence of mouse *Hes5* (−800 ~ +73 bp), pHes3-luc with the promoter sequence of mouse *Hes3* (−2,715 ~ +261 bp) (16), pTP1-luc (pGa 981-6) with an iterated enhancer element with an RBP-J binding site (23), and pEF-BOS-Mam-3-GFP with *MAML2-GFP* fusion gene (8).

Cell Culture—We primarily utilized mouse Leydig tumor (MLT) cells (ATCC, CRL-2065™), which retain the capability to produce testosterone and the responsiveness to human chorionic gonadotropin (hCG) stimulation (24), because *CXorf6* is a causative gene for hypospadias that is predicted to result from impairment of hCG-dependent testosterone production around the critical period for sex development (4, 25) and because the mouse homolog for *CXorf6* is expressed in testosterone-producing Leydig cells (3). We also utilized COS1 cells and HEK293 cells depending on the experimental purposes. These cells were maintained in RPMI 1640 or Dulbecco's modified Eagle's medium supplemented with 10% fetal bovine serum.

Transactivation Analysis of CXorf6—Transactivation function of *CXorf6* was analyzed by the luciferase methods. MLT cells seeded in 6-well dishes ($1.0–1.5 \times 10^5$ cells/well) were transiently transfected using Lipofectamine 2000 (Invitrogen) with 0.6 μg of luciferase reporter vector, 0.6 μg of expression vector for *CXorf6* or *MAML2*, and/or 0.8 μg of expression vector for *N1-ICD* or *N2-ICD*, together with 20 ng of pRL-CMV vector used as an internal control. As controls for the expression vectors, empty counterpart vectors were transfected. Luciferase assays performed with a Lumat LB9507 (Berthold) at 48 h after transfection were repeated 4–5 times.

DNA Binding Analysis of CXorf6—We searched for conserved regions (CRs) between the mouse *Hes3* promoter sequence in the pHes3-luc vector and the human AL031847 sequence containing *HES3* and ~100.2 kb upstream and ~63.8 kb downstream regions using the BLAST data base and performed an electrophoretic mobility shift assay (EMSA) for the CRs using a Lightshift chemiluminescent EMSA kit (Pierce). The procedure was as described in the manufacturer's instructions. In short, MLT cells or COS1 cells cultured in a plate with a diameter of 10 cm were transfected with 5 μg of empty or human *CXorf6* cDNA positive vector, and nuclear extracts were obtained at 48 h after transfection. Then, a small amount of nuclear extracts was incubated with each of biotin-labeled 24–35-bp probes (20 fmol) covering the CRs, and the incubation mixture was subjected to gel electrophoresis. Subsequently, the biotin-labeled probe was detected by chemiluminescence on a nylon membrane.

Western Blot Analysis of CXorf6—Expression vectors for various Myc-tagged CXorf6 proteins (5 μg) were transfected into HEK293 cells in a plate with a diameter of 6 cm. Cell lysates obtained at 48 h after transfection were probed with antibodies for Myc and β-actin utilized as an internal control.

Subcellular Localization Analysis of CXorf6—Subcellular localization of CXorf6 proteins was studied by expressing fusion proteins with RFP or GFP. Vectors for fusion proteins (2

μg) were transfected into MLT cells in a glass dish with a diameter of 3.5 cm. The fluorescent signals were observed at 48–72 h after transfection using a laser-scanning microscope LSM510 (version 3.2; Carl Zeiss) shortly after nuclear staining with 4′,6-diamidino-2-phenylindole.

Nonsense-mediated mRNA Decay (NMD)—Reverse transcriptase (RT)-PCR was performed for two regions of *CXorf6* using lymphoblastoid cell lines of the patient with R653X and his heterozygous mother, with and without the treatment of an NMD inhibitor cycloheximide (CHX) (Sigma; 100 μg/ml, 8-h incubation) (26). The occurrence of NMD was assessed by the presence or absence of the PCR products on the agarose gel in the patient and by the heterozygosity or hemizygosity of the PCR products on the electrochromatograms (CEQ 8000 Autosequencer, Beckman Coulter) in the mother after demonstrating a random X-inactivation pattern by the previously described method (27). Furthermore, maternal RT-PCR products were subcloned with a TOPO TA cloning kit (Invitrogen); 100 clones were subjected to sequencing to confirm the stabilization of mRNA with a nonsense mutation after CHX treatment.

Expression Analysis of HES3/Hes3—Human cDNA samples of penile and genital skin fibroblasts were prepared by RT-PCR using tissues obtained, after receiving permission, from a prepubertal boy with phimosis and from a prepubertal patient with ambiguous genitalia and mutant androgen receptor gene. Other human cDNA samples were purchased from Invitrogen or Clontech. For mouse *Hes3*, RT-PCR was performed for the MLT cells.

Knockdown Analysis for Mouse CXorf6 Homolog—We performed transient knockdown assay for the mouse *CXorf6* homolog using two siRNAs (siRNA1 and siRNA2; final concentration 20 nM). The siRNAs were transfected into MLT cells seeded in 12-well dishes (5×10^4 cells in each well with 1 ml of culture medium, using Lipofectamine RNAimax (Invitrogen). A nontargeting RNA (4611G, Ambion) was similarly transfected as a negative control.

After 48 h of incubation, we the examined mRNA quantity of mouse *CXorf6* homolog in the harvested MLT cells and testosterone concentration in the culture medium using half of the wells. The relative amount of mRNA was determined by the Taqman real-time PCR method using the probe-primer mix for mouse *CXorf6* homolog (assay No. mm01293665_m1, ABI) on an ABI PRISM 7000, using β2-microglobulin for an endogenous control. Testosterone concentration was measured by an electrochemiluminescence immunoassay. In addition, we further analyzed the testosterone production potential of the siRNA-transfected MLT cells in the remaining wells. After changing the old medium with a fresh medium containing hCG (Mochida Pharmaceutical; final concentration, 50 IU/liter), we cultured the cells for a further 1 h and measured testosterone concentration in the medium. These siRNA experiments were performed three times.

SF1 Target Sequence in CXorf6—We searched for a putative SF1 binding site in the genomic sequences of *CXorf6* (AC109994) and the mouse homolog (NT_039706) and performed DNA binding and the transactivation analyses. For the DNA binding analysis, the ^{35}S-labeled 30-bp probes containing the putative SF1 binding site in *CXorf6* were incubated with nuclear extracts of COS1 cells transfected by an empty or human *SF1* cDNA positive vector (pRK5) (Addgene) or with recombinant mouse Sf1 protein and were subjected to gel electrophoresis. Similar analysis was also performed for a 32-bp probe harboring the known SF1 binding site of *CYP11A1* (28) as a control. Furthermore, the biotin-labeled 30-bp probes containing the wild-type or the mutated SF1 binding site were incubated with nuclear extracts of COS1 cells transfected by a human *SF1* cDNA positive vector (pCMX-PL2) and were subjected to gel electrophoresis.

For the transactivation analysis, a fragment (−1,924 ~ −1,690) containing a putative SF1 binding site of *CXorf6* was PCR-amplified and inserted into the pGL3 basic luciferase reporter vector (Promega). Furthermore, a reporter vector carrying the mutation in the putative SF1 binding site was generated by mutagenesis. These reporter vectors (0.5 μg) were transfected into the MLT cells together with the empty or human *SF1* cDNA positive expression vector (2.5 μg) as well as pRL-CMV vector (20 ng) used as an internal control. The luciferase assays were repeated three times.

Statistical Analysis—The results are expressed as the mean ± S.D. and statistical significance was determined by the *t* test. $p < 0.05$ was considered significant.

RESULTS

Structural Analysis of CXorf6 Protein—We found that CXorf6 protein has a unique structure with homology to that of MAML2 protein (Fig. 1*A*). A unique amino acid sequence, which we designated the mastermind-like (MAML) motif, was inferred from sequence alignment with MAML1, MAML2, and MAML3 proteins (8, 9). The MAML motif was well conserved among CXorf6 orthologs identified in frog, bird, and mammals (Fig. 1*B*). In addition, a serine-rich domain was identified in CXorf6, as well as glutamine- and proline-rich domains.

Transcriptional Transactivation by the Wild-type CXorf6 Protein—We examined whether the wild-type CXorf6 (with exon 4) protein is involved in Notch signaling (Fig. 2*A*). Expression of CXorf6 alone slightly but significantly increased the luciferase activity in the absence of *Hes* promoters (pGL2 basic only), probably via some backbone vector sequence. This phenomenon was more evident for other vectors such as pGL3 basic and pGL4 basic (not shown). Thus, we utilized pGL2 basic-based luciferase reporter constructs with the promoter sequences of *Hes1*, *Hes5*, and *Hes3* (16).

For the canonical Notch target genes *Hes1* and *Hes5* with the RBP-J binding site (16), CXorf6 was incapable of enhancing the promoter activities beyond those observed for the pGL2 basic only. MAML2 had no transactivating function, and N-ICDs activated the promoters. The N-ICD-induced promoter activities were further enhanced by CXorf6, probably because of additive or synergic effects via some backbone vector sequence, and by MAML2 because of its co-activator function. The results from the MAML2 and N-ICDs studies were consistent with those reported previously (8, 9, 16).

By contrast, for the noncanonical Notch target gene *Hes3* without the RBP-J binding site (16), CXorf6 alone was capable of enhancing its promoter activity, whereas MAML2 and

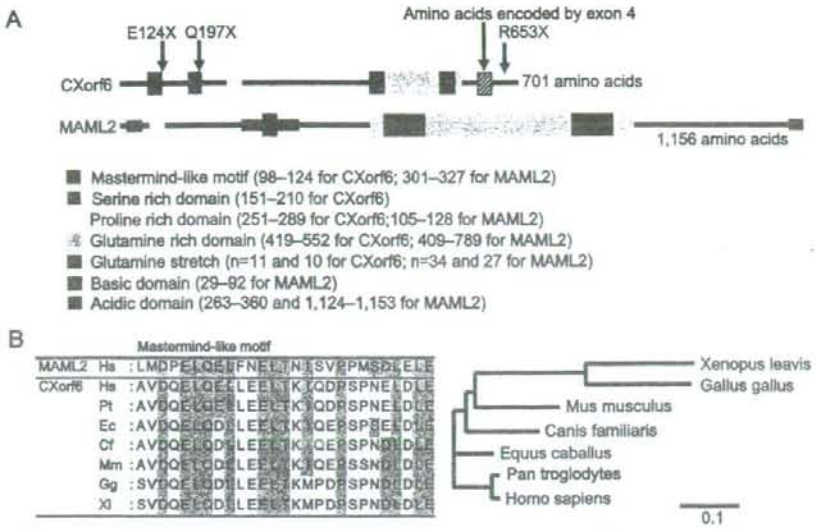

FIGURE 1. **Protein structure analysis.** *A*, the structure of human CXorf6 and MAML2 proteins. The identified domains are shown, together with the positions of the previously reported three nonsense mutations. *B*, amino acid sequence and a phylogenetic tree of the mastermind-like motif. *Hs*, *Homo sapiens* (human); *Pt*, *Pan troglodytes* (chimpanzee); *Ec*, *Equus caballus* (horse); *Cf*, *Canis familiaris* (dog); *Mm*, *Mus musculus* (mouse); *Gg*, *Gallus gallus* (chicken); *Xl*, *Xenopus laevis* (clawed frog). The conserved amino acids are *shaded*. In the phylogenetic tree, the horizontal distance indicates the degree of sequence divergence, and the *scale* represents the number of substitution events (10 per 100 amino acids).

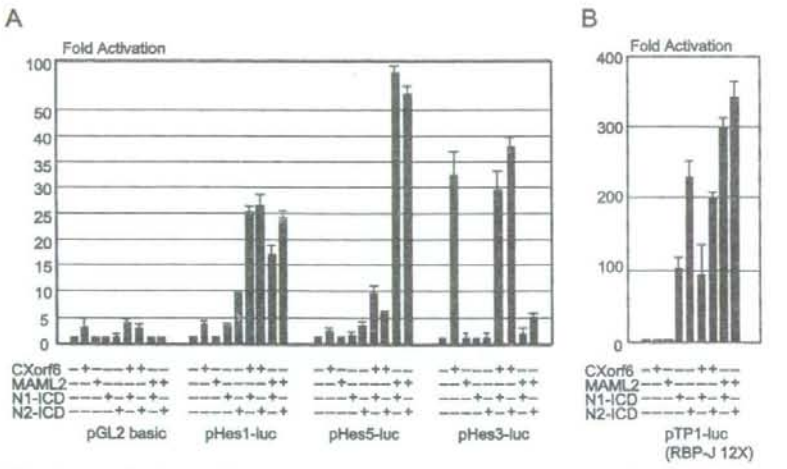

FIGURE 2. **Transactivation functions of the wild-type CXorf6 protein.** *A*, transactivating activities for pGL2 basic vector only and for pHes1-luc, pHes5-luc, and pHes3-luc vectors. The + symbols indicate the presence of expression vectors with cDNAs for *CXorf6*, *MAML2*, *N1-ICD*, and *N2-ICD*, and the − symbols denote the presence of expression vector only (*empty*). *B*, transactivating activities for pTP1-luc.

N-ICDs had no transactivating function. Consistent with this, co-expression of N-ICDs and CXorf6 or MAML2 exhibited no additive or synergic effects on the promoter activity.

These results argue that CXorf6 exerts its transactivation activity independently of the RBP-J binding sites. To confirm this, we performed similar analysis using pTP1-luc, which possesses an iterated enhancer element with an RBP-J binding site (23). As expected, CXorf6 was incapable of enhancing the N-ICD-induced transactivation, whereas MAML2 augmented the N-ICD-induced activities of this promoter (Fig. 2*B*).

DNA Binding Analysis of the Wild-type CXorf6 Protein—We attempted to examine whether the wild-type CXorf6 can bind to the *Hes3* promoter sequence directly (supplemental Fig. 1). Comparison of the 2,976-bp mouse *Hes3* promoter sequence with the human AL031847 sequence identified five CRs (CR1–CR5). Notably, the five CRs found in the human also resided in the upstream of the coding sequences of *HES3*, and the orientation of the CR1–CR5 was well conserved between human and mouse, whereas the mouse *Hes3* promoter region was associated with repeat sequences between CR4 and CR5. EMSA was carried out using 24–35-bp overlapping biotin-labeled probes covering the CR1–CR5 (total, 25 probes), showing no evidence for the DNA-binding capacity of CXorf6.

Transactivation Function of Mutant and Variant CXorf6 Proteins—We next analyzed the transactivating activities of the previously identified three apparently pathologic nonsense mutants and three apparently non-pathologic missense variants of *CXorf6* (3) (Fig. 3*A*) using the pHes3-luc vector. The E124X and Q197X proteins had no transactivation function, whereas the R653X protein as well as the three variant (P286S, Q507R, and N589S) proteins retained a nearly normal transactivating activity (Fig. 3*B*). In addition, the transactivation function was significantly reduced in the L103P protein (an artificially constructed variant affecting the MAML motif) and was normal in ΔExon 4. Transactivation analysis was also performed in the presence of N-ICDs, showing similar results (not shown). Western blot analysis for the three nonsense mutants verified the presence of proteins with expected molecular masses, whereas expression of the E124X protein appeared to be relatively reduced and that of Q197X protein was somewhat increased (Fig. 3*C*).

Subcellular Localization Analysis of Various CXorf6 Proteins—The RFP-CXorf6 (wild-type with exon 4) fusion protein were distributed in a speckled pattern and co-localized with the MAML2-GFP fusion protein (Fig. 4*A*). Furthermore, although the GFP-E124X and GFP-Q197X fusion proteins resided in the

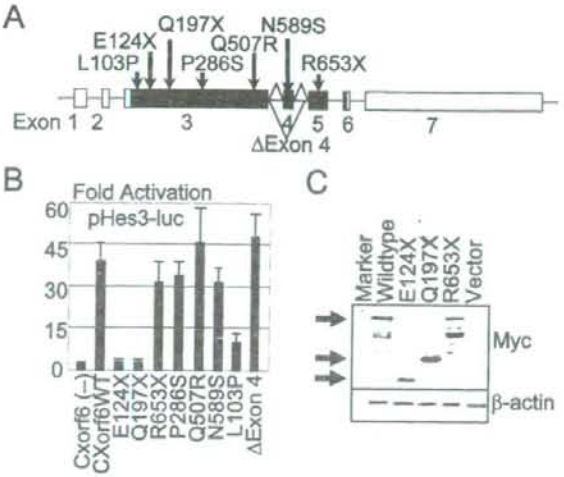

FIGURE 3. **Transactivation functions of the mutant and variant CXorf6 proteins.** *A*, the position of analyzed mutations and variations. L103P is an artificial substitution affecting the MAML motif, and the remaining mutations and variations are naturally occurring substitutions. ΔExon 4 is the minor splice variant lacking exon 4. The *black* and *white areas* denote the coding regions and the untranslated regions, respectively. *B*, transactivating activities of the mutant and variant CXorf6 proteins for the pHes3-luc in the absence of N-ICDs. *C*, Western blot analysis using antibodies for Myc and β-actin.

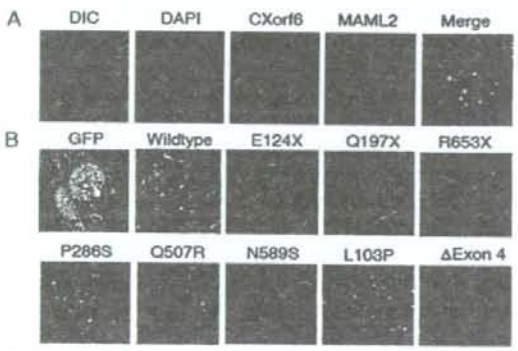

FIGURE 4. **Subcellular localizations of various CXorf6 proteins.** *A*, co-localization of the wild-type CXorf6 and MAML2 in nuclear bodies. Different images of a single cell are shown. The differential interference contrast (*DIC*) microscope image has been utilized for phase contrast, and nuclear counterstaining was performed with 4′,6-diamidino-2-phenylindole (*DAPI*). *B*, appearance of the mutant and the variant CXorf6 proteins after 4′,6-diamidino-2-phenylindole staining.

nucleus, they were incapable of localizing to the nuclear bodies (Fig. 4*B*). The remaining fusion proteins formed between the GFP and CXorf6 mutants and variants including R653X showed a punctate pattern (Fig. 4*B*) and co-localized with the RFP-CXorf6 (wild-type with exon 4) fusion protein (not shown).

Nonsense-mediated mRNA Decay—The above results indicate that the artificially produced R653X protein retains an almost normal function. In this regard, we have shown that R653X, as well as E124X and Q197X, causes NMD *in vivo*, by RT-PCR analysis of leukocytes of the patients (3). Indeed, the positions of these mutations including R653X (1957C > T) satisfy the condition for the occurrence of NMD (29).

To further confirm this event in the R653X mutation, we examined two regions of *CXorf6* mRNA obtained from lymphoblastoid cell lines of the patient and his heterozygous mother, using an NMD inhibitor, CHX (Fig. 5*A*). In the patient, RT-PCR amplification for regions 1 and 2 yielded no or very faint product without CHX treatment and a clear band with CHX treatment (Fig. 5*B*). In the mother, methylation pattern analysis of the androgen receptor gene (exon 1) indicated random X-inactivation (40:60%), and RT-PCR direct sequencing for a part of the region 2 encompassing the mutation delineated only the wild-type allele without CHX treatment and both wild-type and mutant alleles with CHX treatment (Fig. 5*C*). Furthermore, the analysis of 100 maternal RT-PCR clones showed only the wild-type sequence without CHX treatment and both wild-type and mutant sequences with a ratio of 56:44, which is similar to the X-inactivation ratio, after CHX treatment. These findings argue for the occurrence of NMD in the R653X mutation.

Expression Analysis of HES3/Hes3—PCR-based cDNA library screening for *HES3* identified variable degrees of expression in a range of tissues including fetal testis and adult ovary (Fig. 6). In addition, *Hes3* was expressed in the MLT cells (not shown).

Knockdown Analysis for Mouse CXorf6 Homolog—At 48 h after transfection, the mRNA level of the endogenous mouse *CXorf6* homolog was severely reduced in the MLT cells (relative amount: 28% for siRNA1 and 29% for siRNA2), indicating the successful knockdown (Fig. 7*A*). At that time, testosterone concentration was also significantly decreased in the medium harboring the knockdown cells (relative concentration: 63% for siRNA1 and 81% for siRNA2) (Fig. 7*B*). Furthermore, hCG-stimulated testosterone production during a subsequent 1 h was also compromised in the knockdown MLT cells (relative concentration: 53% for siRNA1 and 55% for siRNA2) (Fig. 7*C*).

SF1 Target Sequence in CXorf6—A putative SF1 binding sequence, CCAAGGTCA, was identified at intron 2 upstream of the coding region of *CXorf6* (−1,773 ~ −1,765) (Fig. 8*A*). This binding site was also found at intron 1 in the upstream coding region in the mouse homolog (−42,904 ~ −42,896 and −9,986 ~ −9,978) (not shown). Both human SF1 and mouse Sf1 proteins were capable of binding to the putative SF1 binding site of *CXorf6* as well as to the known SF1 binding site of *CYP11A1* (Fig. 8*B*). This SF1 protein binding was drastically reduced when the putative SF1 binding site CCAAGGTCA was mutated as CCATTGTCA (Fig. 8*C*). Consistent with this finding, although the SF1 protein transactivated the luciferase activity of the wild-type reporter, the transactivation function of SF1 protein was significantly reduced for the mutant reporter (Fig. 8*C*).

DISCUSSION

The wild-type CXorf6 co-localized with structurally related MAML2 in the nuclear bodies and transactivated the *Hes3* promoter without demonstrable DNA-binding capacity. These findings are consistent with transcription usually occurring around nuclear bodies (30, 31) and suggest that CXorf6 may be recruited to the *Hes3* promoter as a non-DNA-binding transcriptional co-activator, although the possibility that CXorf6

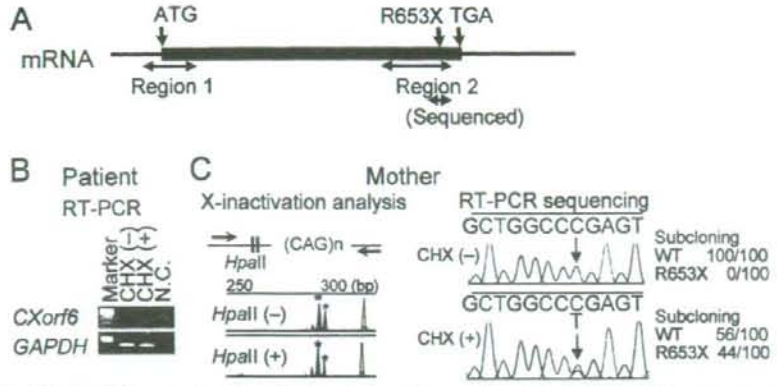

FIGURE 5. **The NMD analysis for the R653X mutation.** *A*, the position of the R653X mutation and the examined regions. Region 1 spans exon 2 to exon 3 and encompasses the start codon. Region 2 spans exon 3 to exon 5 and involves the mutation. The *gray regions* represent the coding region, and the *horizontal line* denotes the untranslated regions. *B*, representative results of the patient. After 40 cycles of RT-PCR for region 1, no band is seen without CHX treatment (CHX(−)), and a clear band is observed after CHX treatment (CHX(+)). *GAPDH*, glyceraldehyde-3-phosphate dehydrogenase gene; *N.C.*, negative control. *C*, representative results of the heterozygous mother. *Left*, X-inactivation analysis for a region encompassing the highly polymorphic CAG repeat tract and two methylation-sensitive HpaII sites at exon 1 of the androgen receptor gene. PCR products are obtained from both active and inactive X chromosomes before HpaII digestion and from inactive X chromosomes only after HpaII digestion. The comparison of the area under the curves between two heterozygous peaks (282 and 285 bp, marked with *asterisks*) before and after the HpaII digestion indicates that the two X chromosomes undergo random X-inactivation with a ratio of 40:60%. The small 276- and 279-bp peaks are byproducts of the slippage phenomenon. *Right*, RT-PCR direct sequencing for a region encompassing the mutation. The normal allele-only is delineated without CHX treatment (−), and the normal and nonsense alleles are identified with CHX treatment (+). The sequencing of 100 RT-PCR clones revealed wild-type clones-only (*WT*) without CHX treatment and both wild-type ($n = 56$) and mutant ($n = 44$) clones after CHX treatment.

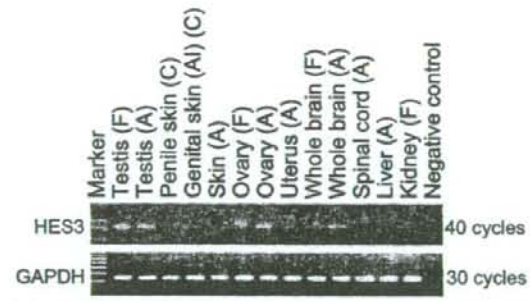

FIGURE 6. **PCR-based human cDNA screening for *HES3*.** The glyceraldehyde-3-phosphate dehydrogenase gene (*GAPDH*) was utilized as an internal control. *F*, fetus; *C*, child; *A*, adult; *AI*, androgen insensitivity.

protein can bind to a non-examined sequence(s) has not been excluded at present. It might be possible, therefore, that *MAML2* and *CXorf6* are distantly related molecules derived from a common ancestor and that *MAML2* has evolved as a co-activator for the RBP-J dependent canonical Notch signaling, whereas *CXorf6* has evolved as a co-activator for the transcription of noncanonical Notch target *Hes3*. In this regard, although MAML2 can augment the endogenous RBP-J-dependent transcription of canonical Notch target genes only in the presence of N-ICD (Refs. 8 and 9 and the present study), CXorf6 alone was capable of enhancing the *Hes3* promoter activity. This would be relevant to CXorf6 being devoid of the N-terminal region of MAML2 including the basic domain, which is essential for the ternary complex formation of MAML2 with N-ICD and RBP-J at the nuclear bodies (8, 9, 12–14), and implies that CXorf6 may directly interact with an unknown endogenous DNA-binding transcription factor for *Hes3*. Although STAT3 may be a candidate DNA-binding transcription factor for *Hes3* (17), there have been no data indicating a STAT3 binding to the *Hes3* promoter in the noncanonical Notch signaling pathway, and *STAT3* is expressed predominantly in the germ cells rather than in the *CXorf6* expression positive Sertoli and Leydig cells in the developing testis (32). Thus, further studies are required to clarify how *CXorf6* transactivates *Hes3* transcription. In addition, there may be other target gene(s) of *CXorf6* besides *Hes3*.

Several domains were identified in the CXorf6 protein in addition to the previously reported glutamine- and proline-rich domains (1). In this regard, the evolutionally conserved MAML motif may play a critical role in the transactivating activity, because the L103P protein had a reduced transactivation function. The serine-rich domain may also be relevant to the transactivation (33). Furthermore, it is inferred that a nuclear localization signal resides on the N-terminal 123 amino acids and a nuclear body localization signal lies on amino acids 197–653, except for amino acids 567–607 encoded by exon 4. It might be possible that a nuclear body localization signal is preserved in the Q197X protein, and in the E124X protein as well, but could not function because of an aberrant protein folding.

Functional studies provided the molecular basis for the previously identified mutations and variations. The E124X and Q197X mutations previously have been shown to undergo NMD (3); if a small amount of truncated proteins were produced by mRNAs escaping NMD, such proteins would be nonfunctional. For the R653X mutation, although the artificially produced truncated protein had a normal transactivation function *in vitro*, the NMD analysis implies the occurrence of nearly complete NMD *in vivo*. The P286S, Q507R, and N589S proteins were confirmed to retain normal functions. These results are consistent with the previous genotype-phenotype correlations of the mutations and variations (3).

The siRNA experiments imply that *CXorf6* is involved in testosterone production. In this context, it appears that testosterone production is not abolished in the absence of residual *CXorf6* expression, because the degree of reduction was more obvious for the mRNA level than for the testosterone concentration. This would be consistent with the development of hypospadias in patients with *CXorf6* nonsense mutations (3), because hypospadias is a phenotype caused by reduced, but not absent, testosterone effects around the critical period for sex development (4, 25). When testosterone effects are abolished,

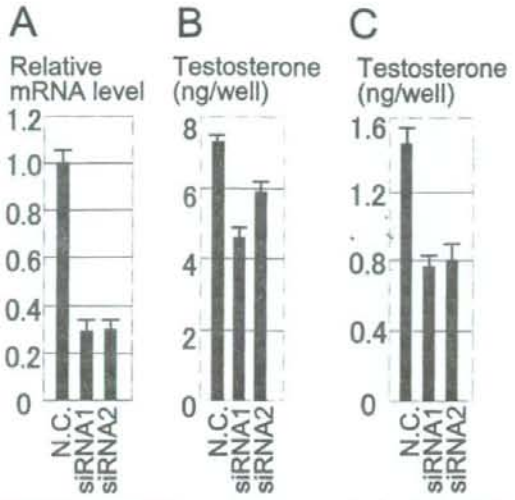

FIGURE 7. **Effects of siRNA on testosterone production in the MLT cells.** *A*, relative mouse *CXorf6* mRNA level in MLT cells after 48 h of incubation with two siRNAs. *B*, testosterone concentration in the medium after 48 h of incubation with two siRNAs. *C*, testosterone concentration in the medium after one h of incubation with hCG, using MLT cells cultured with two siRNA for 48 h. *N.C.*, negative control transfected with nontargeting RNA.

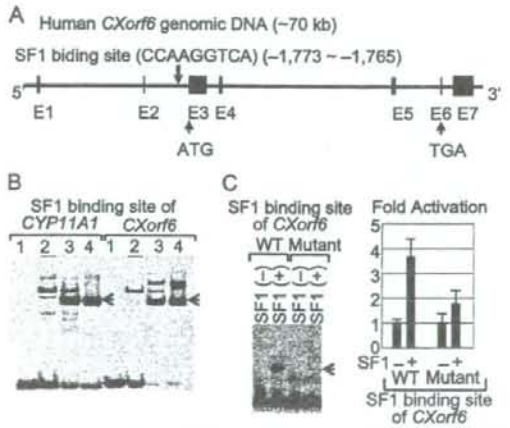

FIGURE 8. **Interaction between *SF1* and *CXorf6*.** *A*, genomic sequence of *CXorf6*. The putative SF1 binding site is present at intron 2 in the upstream of the coding region. The *black areas* indicate exons E1–E7, with the start codon (ATG) on exon 3 and the stop codon (TGA) on exon 6. *B*, EMSA using the ^{35}S-labeled probes containing the previously known SF1 binding site of *CYP11A1* and the putative SF1 binding site of *CXorf6*. *Lane 1*, probe only; *lane 2*, mixture of the probe and nuclear extract of COS1 cells transfected with an empty vector; *lane 3*, mixture of the probe and nuclear extract of COS1 cells transfected with an expression vector with human *SF1* cDNA; *lane 4*, mixture of the probe and recombinant mouse Sf1 protein. *Arrows* indicate the bands retarded due to the binding of the SF1/Sf1 protein. *C*, EMSA and transactivation analysis using wild-type (*WT*) and mutant sequences for the putative SF1 binding site. The binding of SF1 protein to biotin-labeled probes is drastically reduced for the mutant probe (shown by an *arrow*), and the relative luciferase activity is obviously decreased for the reporter with the mutant sequence.

this results in female external genitalia in genetic males (25). Thus, it is likely that *CXorf6* augments testosterone production.

The present study has implications for the molecular network involving *CXorf6*. *HES3* was expressed in the human fetal testis, and the *Hes3* promoter was transactivated by *CXorf6*. *Sf1* is co-expressed with the mouse homolog for *CXorf6* in fetal Sertoli cells and Leydig cells (3), and SF1 transactivated *CXorf6*. Thus, there may be an interaction among *SF1*, *CXorf6*, and *HES3* in the fetal testis, which may play an important role in the testicular function including testosterone production. In this regard, although the mouse homolog for *CXorf6* is not expressed in the adult testis, it is clearly expressed in the adult ovary (3) where *SF1* (4, 5) and *HES3* are also expressed. In addition, premature ovarian failure has been described in a female with heterozygosity for a microdeletion involving *CXorf6* (34). Thus, *CXorf6* and its possible interaction with *SF1* and *HES3* may also be relevant to adult ovarian function.

In summary, the present study implies that *CXorf6* transactivates the *Hes3* promoter, augments testosterone production, and contains the *SF1* target sequence, thereby providing the first clue for the elucidation of the *CXorf6* function. On the basis of the characteristic structure, we have therefore designated *CXorf6* as *MAMLD1*.

Acknowledgments—The reporter vectors pHes1-luc, pHes5-luc, and pHes3-luc were kindly provided by Prof. R. Kageyama, the pEF-BOS-neo-mNotch1 RAMIC vector by Prof. T. Honjo, pEF-BOSneo-aNotch2 by Prof. S. Chiba, pEF-BOS vector by Prof. S. Nagata, Mam-3 cDNA (MAML2, KIAA1819) by Prof. T. Nagase, and pTP1-luc vector by Dr. L. Strobl. We also thank Drs. S. Ikegawa and K. Miyado for technical assistance.

REFERENCES

1. Laporte, J., Kioschis, P., Hu, L. J., Kretz, C., Carlsson, B., Poustka, A., Mandel, J. L., and Dahl, N. (1997) *Genomics* **41,** 458–462
2. Hu, L. J., Laporte, J., Kress, W., Kioschis, P., Siebenhaar, R., Poustka, A., Fardeau, M., Metzenberg, A., Janssen, E. A., Thomas, N., Mandel, J. L., and Dahl, N. (1996) *Hum. Mol. Genet.* **5,** 139–143
3. Fukami, M., Wada, Y., Miyabayashi, K., Nishino, I., Hasegawa, T., Nordenskjöld, A., Camerino, G., Kretz, C., Buj-Bello, A., Laporte, J., Yamada, G., Morohashi, K., and Ogata, T. (2006) *Nat. Genet.* **38,** 1369–1371
4. Baskin, L. S., and Ebbers, M. B. (2007) *J. Pediatr. Surg.* **41,** 463–472
5. Morohashi, K., and Omura, T. (1996) *FASEB J.* **10,** 1569–1577
6. Parker, K. L., and Schimmer, B. P. (1997) *Endocr. Rev.* **18,** 361–377
7. Ozisik, G., Achermann, J.C., and Jameson, J. L. (2002) *Mol. Genet. Metab.* **76,** 85–91
8. Lin, S. E., Oyama, T., Nagase, T., Harigaya, K., and Kitagawa, M. (2002) *J. Biol. Chem.* **277,** 50612–50620
9. Wu, L., Sun, T., Kobayashi, K., Gao, P., and Griffin, J. D. (2002) *Mol. Cell. Biol.* **22,** 7688–7700
10. Artavanis-Tsakonas, S., Rand, M. D., and Lake, R. J. (1999) *Science* **284,** 770–776
11. Iso, T., Kedes, L., and Hamamori, Y. (2003) *J. Cell. Physiol.* **194,** 237–255
12. Tonon, G., Modi, S., Wu, L., Kubo, A., Coxon, A. B., Komiya, T., O'Neil, K., Stover, K., El-Naggar, A., Griffin, J. D., Kirsch, I. R., and Kaye, F. J. (2003) *Nat. Genet.* **33,** 208–213
13. Nam, Y., Sliz, P., Song, L., Aster, J. C., and Blacklow, S. C. (2006) *Cell* **124,** 973–983
14. Wilson, J. J., and Kovall, R. A. (2006) *Cell* **124,** 985–996
15. Sasai, Y., Kageyama, R., Tagawa, Y., Shigemoto, R., and Nakanishi, S. (1992) *Genes Dev.* **6,** 2620–2634
16. Nishimura, M., Isaka, F., Ishibashi, M., Tomita, K., Tsuda, H., Nakanishi, S., and Kageyama, R. (1998) *Genomics* **49,** 69–75
17. Androutsellis-Theotokis, A., Leker, R. R., Soldner, F., Hoeppner, D. J., Ravin, R., Poser, S. W., Rueger, M. A., Bae, S. K., Kittappa, R., and McKay, R. D. (2006) *Nature* **442,** 823–826
18. Thompson, J. D., Gibson, T. J., Plewniak, F., Jeanmougin, F., and Higgins, D. G. (1997) *Nucleic Acids Res.* **25,** 4876–4882

19. Page, R. D. (1996) *Comput. Appl. Biosci.* **12,** 357–358
20. Mizushima, S., and Nagata, S. (1990) *Nucleic Acids Res.* **18,** 5322
21. Mizutani, T., Taniguchi, Y., Aoki, T., Hashimoto, N., and Honjo, T. (2001) *Proc. Natl. Acad. Sci. U. S. A.* **98,** 9026–9031
22. Shimizu, K., Chiba, S., Saito, T., Kumano, K., Hamada, Y., and Hirai, H. (2002) *Biochem. Biophys. Res. Commun.* **291,** 775–779
23. Minoguchi, S., Taniguchi, Y., Kato, H., Okazaki, T., Strobl, L. J., Zimber-Strobl, U., Bornkamm, G. W., and Honjo, T. (1997) *Mol. Cell. Biol.* **17,** 2679–2687
24. Panesar, N. S., Chan, K. W., and Ho, C. S. (2003) *Steroids* **68,** 245–251
25. Grumbach, M. M., Hughes, I. A., and Conte, F. A. (2002) in *Williams Textbook of Endocrinology* (Larsen, P. R., Kronenberg, H. M., Melmed, S., and Polonsky, K. S., eds) 10th Ed., pp. 842–962, Saunders, Philadelphia
26. Freddi, S., Savarirayan, R., and Bateman, J. F. (2000) *Am. J. Med. Genet.* **90,** 398–406
27. Muroya, K., Kosho, T., Matsuo, M., and Ogata, T. (1999) *Am. J. Med. Genet.* **84,** 384–385
28. Liu, Z., and Simpson, E. R. (1997) *Mol. Endocrinol.* **11,** 127–137
29. Kuzmiak, H. A., and Maquat, L. E. (2006) *Trends Mol. Med.* **12,** 306–316
30. Zhong, S., Salomoni, P., and Pandolfi, P. P. (2000) *Nat. Cell Biol.* **2,** E85–E90
31. Wu, L., Aster, J. C., Blacklow, S. C., Lake, R., Artavanis-Tsakonas, S., and Griffin, J. D. (2000) *Nat. Genet.* **26,** 484–489
32. Murphy, K., Carvajal, L., Medico, L., and Pepling, M. (2005) *Gene Expr. Patterns* **5,** 475–482
33. Nowling, T. K., Johnson, L. R., Wiebe, M. S., and Rizzino, A. (2000) *J. Biol. Chem.* **275,** 3810–3818
34. Bartsch, O., Kress, W., Wagner, A., and Seemanova, E. (1999) *Cytogenet. Cell Genet.* **85,** 310–314

J Hum Genet (2008) 53:454–459
DOI 10.1007/s10038-008-0269-z

ORIGINAL ARTICLE

Identification and characterization of cryptic *SHOX* intragenic deletions in three Japanese patients with Léri–Weill dyschondrosteosis

Maki Fukami · Sumito Dateki · Fumiko Kato · Yukihiro Hasegawa · Hiroshi Mochizuki · Reiko Horikawa · Tsutomu Ogata

Received: 25 December 2007 / Accepted: 11 February 2008 / Published online: 6 March 2008
© The Japan Society of Human Genetics and Springer 2008

Abstract Although short-stature homeobox-containing gene (*SHOX*) haploinsufficiency is responsible for Léri–Weill dyschondrosteosis (LWD), the molecular defect has not been identified in ~20% of Japanese LWD patients. Furthermore, although high prevalence of microdeletions affecting *SHOX* is primarily ascribed to the presence of repeat sequences such as *Alu* elements around *SHOX*, it remains to be determined whether microdeletions are actually mediated by repeat sequences. We performed multiple ligation probe amplification (MLPA) assay in six Japanese LWD patients with apparently normal *SHOX*, followed by fluorescent in situ hybridization (FISH) analysis and sequencing for polymerase chain reaction (PCR) products encompassing the deletion junctions in patients with abnormal MLPA patterns. Consequently, heterozygous intragenic deletions were identified in three cases, i.e., a 5,906-bp deletion involving exons 4–5 in case 1, a 5,594-bp deletion involving exons 4–6a in case 2, and a 50,199-bp deletion involving exons 4–6b in case 3. The deletion breakpoints of cases 1 and 2 were present in nonrepeat sequences, whereas those of case 3 resided within *Alu* elements. The results suggest that cryptic *SHOX* intragenic deletions account for a small fraction of LWD and that microdeletions affecting *SHOX* can be generated by repeat-sequence-mediated aberrant recombinations and by nonhomologous end joining.

Keywords *SHOX* · Intragenic deletion · MLPA · Léri–Weill dyschondrosteosis · Repeat sequence

M. Fukami (✉) · S. Dateki · F. Kato · T. Ogata
Department of Endocrinology and Metabolism,
National Research Institute for Child Health and Development,
2-10-1 Ohkura, Setagaya, Tokyo 157-8535, Japan
e-mail: mfukami@nch.go.jp

S. Dateki
Department of Pediatrics, Nagasaki University
School of Medicine, Nagasaki, Japan

Y. Hasegawa
Endocrinology and Metabolism Unit, Tokyo Metropolitan
Kiyose Children's Hospital, Tokyo, Japan

H. Mochizuki
Department of Endocrinology and Metabolism,
Saitama Children's Medical Center, Saitama, Japan

R. Horikawa
Division of Endocrinology and Metabolism,
National Center for Child Health and Development,
Tokyo, Japan

Introduction

Léri–Weill dyschondrosteosis (LWD) is a dominantly inherited skeletal dysplasia characterized by Madelung deformity and mesomelic short stature (Langer 1965). It is caused by haploinsufficiency of the short-stature homeobox-containing gene (*SHOX*) on the short arm pseudoautosomal region (PAR1) of the human sex chromosomes (Ogata 2002; Blaschke and Rappold 2006). To date, extensive studies have been performed, identifying multiple intragenic mutations (Niesler et al. 2007) and various submicroscopic deletions encompassing the entire *SHOX* coding region and/or the putative downstream enhancer region(s) (Kosho et al. 1999; Ogata 2002; Benito-Sanz et al. 2005, 2006a, b; Fukami et al. 2006; Huber et al. 2006; Sabherwal et al. 2007). Submicroscopic deletions are more frequent than intragenic mutations (Ogata 2002), and this would be consistent with repeat sequences being

abundantly present around *SHOX*, because aberrant intrachromosomal or interchromosomal recombinations are prone to occur between such sequences (Ogata 2002; Blaschke and Rappold 2006). Indeed, *Alu* and L1 elements are abundant on the X chromosome, with *Alu* elements being more frequent and L1 elements being less frequent on the PAR1 than on the rest of the X chromosome (Lyon 2000; Blaschke and Rappold 2006). However, *SHOX* abnormalities have not been identified in a substantial fraction of LWD patients (Benito-Sanz et al. 2006a; Blaschke and Rappold 2006), and we have also failed to reveal *SHOX* abnormalities in ~20% of Japanese LWD patients (Ogata 2002). Furthermore, it remains to be determined whether microdeletions around *SHOX* are directly mediated by repeat sequences.

Multiple ligation probe amplification (MLPA) is a recently developed method for relative quantification of single-copy sequences in the human genome (Schouten et al. 2002). It has been demonstrated as a powerful tool in the detection of deletions affecting several genes, including *SHOX* (Benito-Sanz et al. 2005, 2006a, b; Gatta et al. 2007). However, except for a single patient with a tiny deletion encompassing exons 4–6a of *SHOX* that could be revealed only by MLPA analysis (Benito-Sanz et al. 2006b), this method has been performed in patients with sex chromosomal abnormalities or relatively large deletions involving the entire *SHOX* coding region and/or the downstream enhancer region(s) that can be identified by other methods such as fluorescent in situ hybridization (FISH) analysis and microsatellite genotyping (Kosho et al. 1999; Benito-Sanz et al. 2006a, b; Gatta et al. 2007).

Here we report three cryptic *SHOX* intragenic deletions that were first identified by MLPA analysis. Characterization of deletions implies that microdeletions affecting *SHOX* can be generated by homologous and nonhomologous rearrangements.

Patients and methods

Patients

We studied six unrelated Japanese female patients (cases 1–6) with definitive LWD phenotype [Madelung deformity and mesomelic short stature ranging from −4.4 standard deviation (SD) to −2.0 SD] in whom *SHOX* abnormality was not demonstrated by direct sequencing of coding exons 2–6b, by FISH analysis with an ~18-kb cosmid probe spanning from intron 2 to intron 6a (Kosho et al. 1999), and by microsatellite and single nucleotide polymorphism (SNP) genotyping for previously described multiple loci utilized for localizing downstream enhancer(s) (Benito-Sanz et al. 2005; Fukami et al. 2006; Huber et al. 2006).

MLPA analysis

This study was approved by the Institutional Review Board Committee at the National Center for Child Health and Development. After taking informed consent, MLPA was performed for cases 1–6 and three control female subjects using a SALSA MLPA Kit P018B (MRC-Holland, Amsterdam, the Netherlands) that contains probes for various parts of *SHOX* (*SHOX*-specific probes) (Fig. 1a) and multiple other loci (reference probes). The protocol was as described in the manufacturer's instructions (Schouten et al. 2002). In brief, 50 ng of leukocyte genomic DNA was hybridized with the probe mix, and the hybridization mixture was subjected to ligase reaction and polymerase chain rection (PCR) amplification. Subsequently, the PCR products amplified from ligated probes were visualized on a 310 ABI PRISM genetic analyzer (ABI Prisms, Foster City, CA, USA). For each *SHOX*-specific probe, a relative peak area was calculated by dividing each measured peak area by the sum of peak areas of the reference probes. The relative areas were compared between cases and controls, and relative peak areas less than 65% of those of controls were assessed to be indicative of heterozygous deletions (Schouten et al. 2002; Kozak et al. 2006).

FISH analysis

FISH was performed with probes detecting the presumably deleted regions indicated by MLPA. The probes were obtained by long PCR using LA taq polymerase (Takara, Ohtsu) and were labeled with digoxigenin and detected by rhodamine antidigoxigenin. A SpectrumGreen-labeled probe for *DXZ1* (Abbott, Abbott Park, IL, USA) was utilized as an internal control. For comparison, FISH was also performed with the cosmid probe (Fig. 1a) using previously described methods (Kosho et al. 1999).

Characterization of the deletions

Long PCR was performed with multiple primer pairs flanking the deleted regions. When long PCR products were obtained, they were subjected to direct sequencing using serial primers. The deletion size and the junction structure were determined by comparing the obtained sequences with the BX004827 and AL683871 sequences [National Center for Biotechnology Information (NCBI) database]. The presence or absence of repeat sequences around the breakpoints was examined with Repeatmasker (http://www.repeatmasker.org).

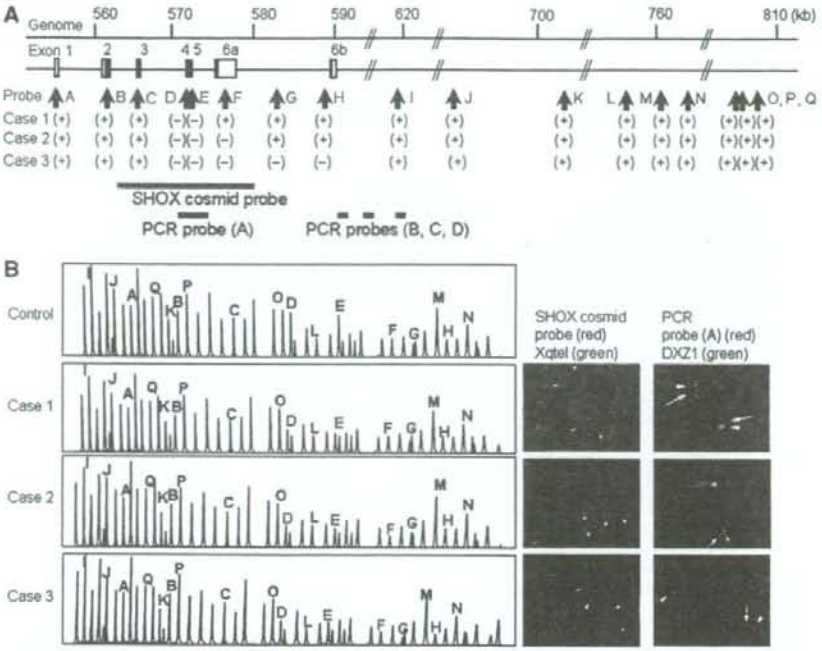

Fig. 1 Identification of cryptic intragenic short-stature homeobox-containing gene (*SHOX*) deletions in cases 1–3. **a** Summary of the multiple ligation probe amplification (MLPA) analyses and the fluorescent in situ hybridization (FISH) probes utilized in this study. The *upper horizontal line* indicates the physical distance from the Xp/Yp telomere. The *rectangles* represent *SHOX* exons (1–6b); the *black* and *white areas* denote the coding regions and the untranslated regions, respectively. The sites examined by MLPA probes (*A–Q*) are indicated by *arrows*; of these, the *A–F* sites reside on exons 1–6a, the *H* site lies just upstream of exon 6b, and thr *I–Q* sites reside around the enhancer region postulated at a position 30–250 kb downstream of *SHOX* coding region. The *plus* and the *minus symbols* represent the presence of two copies and a single copy of the corresponding sites, respectively. The *lower thick lines* represent the regions detected by FISH probes. The previously reported *SHOX* cosmid probe (Kosho et al. 1999) detects a ~18-kb region from intron 2 to intron 6a, polymerase chain reaction (PCR) probe *A* detects a ~4.0-kb region from intron 3 to intron 5, PCR probe *B* detects a ~5.2-kb region just proximal to exon 6b, PCR probe *C* detects a ~5.6-kb region at a position ~19-kb proximal to exon 6b, and PCR probe *D* detects a ~5.3-kb region at a position ~32-kb proximal to exon 6b. The primers utilized were 5′-TCTCTCTCTGCTTCTCCCCA-3′ and 5′-GTGCAGGACGCGCGGT-3′ for PCR probe A, 5′-GTTAATGC TGAGAAGCTCTCCAAGCTAC-3′ and 5′-GTCCCTTACAAGGAC ACCTGTTATTGGAT-3′ for PCR probe B, 5′-GCTTGGTAGGAA GAGCCACAACTGTTCA-3′ and 5′-CTAGACGTCCACGGACCT ATGTTGTAAC-3′ for PCR probe C, and 5′-TGAGTAATTAAT CCCCACCAGTGAGGTC-3′ and 5′-CGTAGTTGGCCAAGACTC CACCATATTG-3′ for PCR probe D. **b** Results of MLPA assays (*left part*) and FISH analyses (*right part*). The *peaks* corresponding to sites around *SHOX* are indicated (*A–Q*); of these, the *A–F* sites reside on exons 1–6a, the *H* site lies just upstream of exon 6b, and *I–Q* sites reside around the enhancer region postulated at a position 30–250 kb downstream of *SHOX* coding region. MLPA assays indicate that compared with the relative peak areas in control female subjects, the relative peak areas for *D* and *E* in case 1, those for *D–F* in case 2, and those for *D–H* in case 3 are significantly reduced (shown in *red*). Relative peak areas for other loci (not specifically indicated) are similar between control female subjects and cases 1–3. The *red peaks* indicate the internal size markers. FISH analysis demonstrates that the ~4-kb PCR probe A detects one faint and one clear signal in case 1 and only a single signal in cases 2 and 3, whereas the ~18-kb cosmid probe detects two signals in cases 1–3

Results

MLPA analysis

Cryptic *SHOX* intragenic deletions were detected in cases 1–3 (Fig. 1b). Comparisons of relative peak areas indicated heterozygous deletion involving exons 4 and 5 in case 1, that involving exons 4–6a in case 2, and that involving exons 4–6b in case 3. No deletion was identified in cases 4–6. The results were reproduced in two independent experiments.

FISH analysis

FISH was performed with a PCR probe (A) for a region from intron 3 to intron 5 (Fig. 1a), detecting two signals with a marked difference in intensity (apparently one normal and one faint signal) in case 1 and only a single

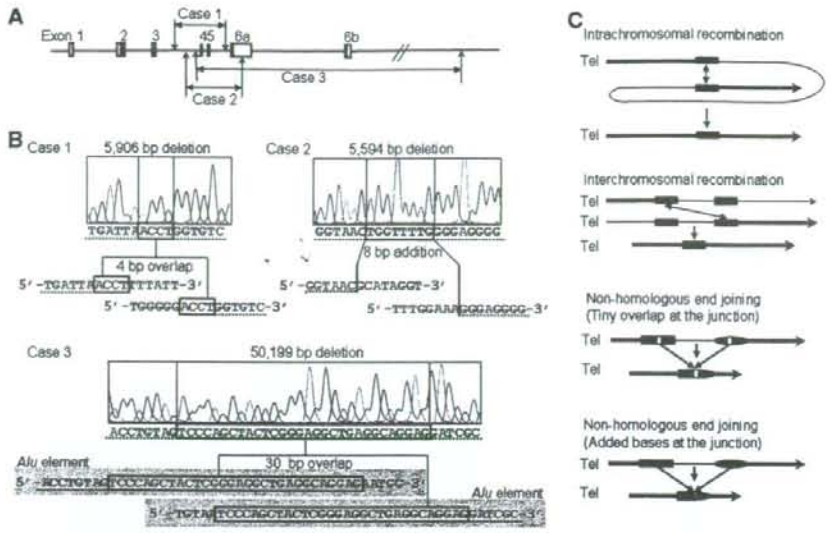

Fig. 2 Deletion sizes and junction structures. **a** Schematic representation of the intragenic deletions in cases 1–3. **b** Electrochromatograms showing the fusion points of the intragenic deletions. In case 1, a 4-bp segment surrounded by a *rectangle* is shared by the distal and the proximal breakpoint sequences. In case 2, an 8-bp segment of unknown origin surrounded by a *rectangle* is added to the deletion junction. In case 3, a 30-bp segment surrounded by a *rectangle* is shared by the distal and proximal breakpoint sequences. The breakpoints in cases 1 and 2 reside in nonrepeat sequences, whereas those in case 3 are present within *Alu* elements (shaded in *light blue*). Polymerase chain reaction (PCR) products encompassing the deletion junctions were obtained with the following primers: 5′-AAATTGGTTGTGGGGTGTGT-3′ and 5′-GTGCAGGACGCGC GG-3′ in case 1, 5′-TGGATCGTGAATCACTCCAA-3′ and 5′-GCCATCTCTACACCCGTGAT-3′ in case 2, and 5′-AACAGA GGTGAAGTGGATAATTGAG-3′ and 5′-TGGTTGGTTAGGAAC TTGAATAGAG-3′ in case 3. The deletion junction sequences were determined with the following primers: 5′-AAATTGGTTGT GGGGTGTGT-3′in case 1, 5′-TTCGGTTCTCCTACAGGGTCT-3′ in case 2, and 5′-GCTAGGTGTGGTGGTGTGC-3′ in case 3. **c** Schematic representation of mechanisms leading to the generation of microdeletions. An aberrant intrachromosomal or interchromosomal recombination mediated by repeat sequences (*green rectangles*) causes a microdeletion (loss of a chromosomal region depicted by *thin lines*) between the repeat sequences. Nonhomologous end joining between nonrepeat sequences (*a blue rectangle and a red ellipse*) yields a microdeletion (*thin lines*) between the nonrepeat sequences and is often associated with an addition of a short segment of unknown origin (*a green segment*) or with a tiny overlapping segment common to the nonhomologous sequences (*yellow segments*)

signal in cases 2 and 3 (Fig. 1b). In case 3 with a relatively large deletion, FISH was further carried out with three PCR probes (B, C, D), localizing the proximal breakpoint between the regions identified by PCR probes C and D (not shown). These microdeletions were not identified by the cosmid probe (Fig. 1b), as mentioned in "Patients".

Deletion characterization

After examination with multiple primer sets, PCR products harboring the deletion junctions were obtained, and the deletion junction sequence was determined in cases 1–3 (Fig. 2a, b). Deletion size was 5,906-bp in case 1, 5,594-bp in case 2, and 50,199-bp in case 3. The deletion breakpoints of cases 1 and 2 were present on nonrepeat sequences, whereas those of case 3 resided within *Alu* elements. The fusion point resided at a 4-bp segment in case 1 and at a 30-bp segment in case 3 and was associated with an addition of an 8-bp segment of unknown origin in case 2.

Discussion

MLPA analysis identified cryptic *SHOX* intragenic deletions in cases 1–3. Since the cryptic deletions were detected in three of the six LWD patients with apparently normal *SHOX*, such tiny intragenic deletions may also be hidden in a substantial fraction of LWD patients without demonstrable *SHOX* haploinsufficiency. In this context, microdeletions affecting *SHOX* are frequently observed in LWD (Ogata 2002), and MLPA can identify at once various types of microdeletions affecting *SHOX*, including those involving a single or a few exons and those involving the entire coding region and/or the downstream enhancer region(s) (Benito-Sanz et al. 2006a, b), using genomic DNA of patients only. Thus, in conjunction with its simple and easy procedure, MLPA will serve as a powerful screening method for *SHOX* molecular defects.

The deletion junction resided in nonrepeat sequences in cases 1 and 2 and within *Alu* elements in case 3. The

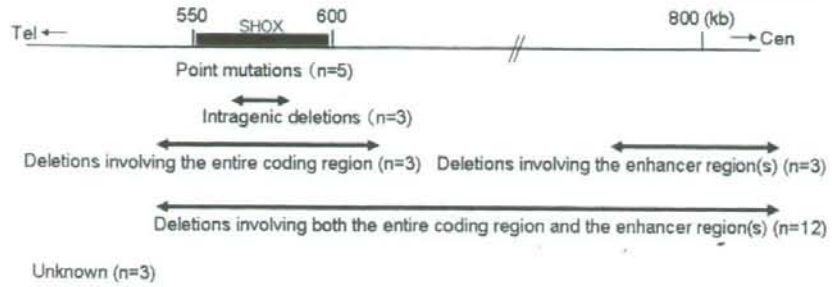

Fig. 3 Short-stature homeobox-containing gene (*SHOX*) abnormalities in 29 Japanese families with Léri–Weill dyschondrosteosis (LWD) and a normal karyotype. The *upper horizontal line* indicates the physical distance from the Xp/Yp telomere ("*Tel*"). The *rectangles* represent *SHOX* coding region. The *black arrows* denote the deleted regions. *SHOX* molecular defects were not identified in three families

intragenic deletion in case 3 would be ascribed to an aberrant intrachromosomal or interchromosomal recombination mediated by repeat sequences (Fig. 2c) (Ogata 2002; Blaschke and Rappold 2006). By contrast, the intragenic deletions in cases 1 and 2 would be due to nonhomologous end joining (NHEJ), i.e., an aberrant breakage and re-union between nonhomologous sequences (Fig. 2c) (Shaw et al. 2004). In particular, the presence of a short segment of unknown origin at the deletion junction in case 2 is characteristic of NHEJ (Shaw et al. 2004). Furthermore, while a short segment common to distal and proximal breakpoint sequences was identified at the deletion junction in case 1, the segment appears to be too short to permit an aberrant recombination, and NHEJ associated with such a tiny overlapping segment has been reported previously (Kozak et al. 2006). In addition, the scattered distribution of the microdeletion breakpoints around *SHOX* (Kosho et al. 1999; Benito-Sanz et al. 2005, 2006a, b; Fukami et al. 2006; Huber et al. 2006; Sabherwal et al. 2007) may primarily reflect genomic rearrangements caused by NHEJ, and NHEJ may be facilitated by the high recombination frequency in the PAR1 and by the abundant presence of repeat sequences (e.g., *Alu* elements) (Shaw et al. 2004; Blaschke and Rappold 2006). Collectively, the present study implies that the microdeletions affecting *SHOX* can be caused by both homologous and nonhomologous rearrangements.

To date, we have examined a total of 29 families containing at least one patient with LWD and a normal karyotype (total 50 patients). Consequently, we identified various types of *SHOX* abnormalities in 26 of the 29 families (~90%), i.e., 12 microdeletions involving the entire coding region and the putative downstream enhancer region(s), three microdeletions involving the entire coding region alone, three microdeletions involving the enhancer region(s) alone, three intragenic deletions, and five intragenic mutations (Kosho et al. 1999; Ogata 2002; Fukami et al. 2006; unpublished data) (Fig. 3). The frequency of *SHOX* abnormalities is higher than that reported by other groups (50–90%) (Blaschke and Rappold 2006). In particular, Benito-Sanz et al. (2006a) detected *SHOX* abnormalities only in 16 of 26 Spanish probands after performing extensive analysis, including MLPA analysis. Although the cause of the difference in the frequency of *SHOX* abnormalities (especially deletions) remains to be examined, this could be due to ethnic differences. Indeed, deletions encompassing *NSD1* for Sotos syndrome are also much more frequently identified in Japanese than in other ethnic groups (Kurotaki et al. 2003).

SHOX molecular defects has not been demonstrated so far in cases 4–6. There are two possible explanations for this. First, there still may be a hidden abnormality impairing *SHOX*. For example, a mutation or a tiny deletion may exist in the promoter region, the nonexamined exonic sequences (MLPA examines only a part of exonic sequences), the intronic sequences, or the enhancer sequences. Second, there may be a mutation in some gene(s) other than *SHOX*. In this regard, one possible locus may reside near the *HOXD* gene cluster. An association between LWD-like skeletal abnormality and a balanced translocation t(2;8)(q31;p21) has been found in a father and his three children, with the 2q31 breakpoint being mapped near the *HOXD* gene cluster (Spitz et al. 2002), and chromosomal breakage around the *HOXD* cluster is known to result in various limb malformations (Dlugaszewska et al. 2006).

In summary, the results suggest that MLPA analysis is a highly useful method to identify microdeletions affecting *SHOX*, including cryptic intragenic deletions, and that such microdeletions can be caused by homologous sequence-mediated aberrant recombinations and by nonhomologous end joining. Further studies will permit re-evaluation of the prevalence of *SHOX* molecular defects and the mechanisms leading to microdeletions affecting *SHOX*.

Acknowledgments We thank Professor Gudrun Rappold, Heidelberg University, for her critical comments, and Mr. Shunji Yamamori, Mitsubishi Chemical Medience Corporation, Tokyo, Japan, for his technical assistance in FISH analysis. This study was supported by Grants for Child Health and Development (17C-2) and for Research on Children and Families (H18-005) from the Ministry of Health, Labor, and Welfare, and by Grants-in-Aid for Scientific Research (category C: 18591178) from the Ministry of Education, Culture, Sports, Science and Technology.

References

Benito-Sanz S, Thomas NS, Huber C, Gorbenko del Blanco D, Aza-Carmona M, Crolla JA, Maloney V, Rappold G, Argente J, Campos-Barros A, Cormier-Daire V, Heath KE (2005) A novel class of Pseudoautosomal region 1 deletions downstream of SHOX is associated with Leri–Weill dyschondrosteosis. Am J Hum Genet 77:533–544

Benito-Sanz S, del Blanco DG, Aza-Carmona M, Magano LF, Lapunzina P, Argente J, Campos-Barros A, Heath KE (2006a) PAR1 deletions downstream of SHOX are the most frequent defect in a Spanish cohort of Leri–Weill dyschondrosteosis (LWD) probands. Hum Mutat 27:1062

Benito-Sanz S, Gorbenko del Blanco D, Huber C, Thomas NS, Aza-Carmona M, Bunyan D, Maloney V, Argente J, Cormier-Daire V, Campos-Barros A, Heath KE (2006b) Characterization of SHOX deletions in Leri–Weill dyschondrosteosis (LWD) reveals genetic heterogeneity and no recombination hotspots. Am J Hum Genet 79:409–414

Blaschke RJ, Rappold G (2006) The pseudoautosomal regions, SHOX and disease. Curr Opin Genet Dev 16:233–239

Dlugaszewska B, Silahtaroglu A, Menzel C, Kubart S, Cohen M, Mundlos S, Tumer Z, Kjaer K, Friedrich U, Ropers HH, Tommerup N, Neitzel H, Kalscheuer VM (2006) Breakpoints around the HOXD cluster result in various limb malformations. J Med Genet 43:111–118

Fukami M, Kato F, Tajima T, Yokoya S, Ogata T (2006) Transactivation function of an approximately 800-bp evolutionarily conserved sequence at the SHOX 3′ region: implication for the downstream enhancer. Am J Hum Genet 78:167–170

Gatta V, Antonucci I, Morizio E, Palka C, Fischetto R, Mokini V, Tumini S, Calabrese G, Stuppia L (2007) Identification and characterization of different SHOX gene deletions in patients with Leri–Weill dyschondrosteosys by MLPA assay. J Hum Genet 52:21–27

Huber C, Rosilio M, Munnich A, Cormier-Daire V, French SHOX GeNeSIS Module (2006) High incidence of SHOX anomalies in individuals with short stature. J Med Genet 43:735–739

Kosho T, Muroya K, Nagai T, Fujimoto M, Yokoya S, Sakamoto H, Hirano T, Terasaki H, Ohashi H, Nishimura G, Sato S, Matsuo N, Ogata T (1999) Skeletal features and growth patterns in 14 patients with haploinsufficiency of SHOX: implications for the development of Turner syndrome. J Clin Endocrinol Metab 84:4613–4621

Kozak L, Hrabincova E, Kintr J, Horky O, Zapletalova P, Blahakova I, Mejstrik P, Prochazkova D (2006) Identification and characterization of large deletions in the phenylalanine hydroxylase (PAH) gene by MLPA: evidence for both homologous and non-homologous mechanisms of rearrangement. Mol Genet Metab 89:300–309

Kurotaki N, Harada N, Shimokawa O, Miyake N, Kawame H, Uetake K, Makita Y, Kondoh T, Ogata T, Hasegawa T, Nagai T, Ozaki T, Touyama M, Shenhav R, Ohashi H, Medne L, Shiihara T, Ohtsu S, Kato Z, Okamoto N, Nishimoto J, Lev D, Miyoshi Y, Ishikiriyama S, Sonoda T, Sakazume S, Fukushima Y, Kurosawa K, Cheng JF, Yoshiura K, Ohta T, Kishino T, Niikawa N, Matsumoto N (2003) Fifty microdeletions among 112 cases of Sotos syndrome: low copy repeats possibly mediate the common deletion. Hum Mutat 22:378–387

Langer LO Jr (1965) Dyschondrosteosis, a heritable bone dysplasia with characteristic roentgenographic features. AJR Am J Roentgenol 95:178–188

Lyon MF (2000) LINE-1 elements and X chromosome inactivation: a function for "junk" DNA? Proc Natl Acad Sci USA 97:6248–6249

Niesler B, Röth R, Wilke S, Fujimura F, Fischer C, Rappold G (2007) The novel Human *SHOX* allelic variant database. Hum Mutat 28:933–938

Ogata T (2002) SHOX haploinsufficiency: lessons from clinical studies. Curr Opin Endocrinol Diabetes 9:13–20

Sabherwal N, Bangs F, Roth R, Weiss B, Jantz K, Tiecke E, Hinkel GK, Spaich C, Hauffa BP, van der Kamp H, Kapeller J, Tickle C, Rappold G (2007) Long-range conserved non-coding SHOX sequences regulate expression in developing chicken limb and are associated with short stature phenotypes in human patients. Hum Mol Genet 16:210–222

Schouten JP, McElgunn CJ, Waaijer R, Zwijnenburg D, Diepvens F, Pals G (2002) Relative quantification of 40 nucleic acid sequences by multiplex ligation-dependent probe amplification. Nucleic Acids Res 30:e57

Shaw CJ, Lupski JR (2004) Implications of human genome architecture for rearrangement-based disorders: the genomic basis of disease. Hum Mol Genet 13(Spec No 1):R57–R64

Spitz F, Montavon T, Monso-Hinard C, Morris M, Ventruto ML, Antonarakis S, Ventruto V, Duboule D (2002) A t(2;8) balanced translocation with breakpoints near the human HOXD complex causes mesomelic dysplasia and vertebral defects. Genomics 79:493–498

European Journal of Human Genetics (2008) 16, 1019–1023
© 2008 Nature Publishing Group All rights reserved 1018-4813/08 $30.00
www.nature.com/ejhg

SHORT REPORT

Epimutation (hypomethylation) affecting the chromosome 14q32.2 imprinted region in a girl with upd(14)mat-like phenotype

Kana Hosoki[1], Tsutomu Ogata*[,2], Masayo Kagami[2], Touju Tanaka[3] and Shinji Saitoh[1]

[1]*Department of Pediatrics, Hokkaido University Graduate School of Medicine, Sapporo, Japan;* [2]*Department of Endocrinology and Metabolism, National Research Institute for Child Health and Development, Tokyo, Japan;* [3]*Division of Clinical Genetics and Molecular Medicine, National Center for Child Health and Development, Tokyo, Japan*

Maternal uniparental disomy for chromosome 14 (upd(14)mat) causes clinically discernible features such as pre- and/or postnatal growth failure, hypotonia, obesity, small hands, and early onset of puberty. The monoallelic expression patterns at the 14q32.2 imprinted region are tightly related to methylation status of the *DLK1–MEG3* intergenic differential methylation region (DMR) and the *MEG3*-DMR that are severely hypermethylated after paternal transmission and grossly hypomethylated after maternal transmission. We examined this imprinted region in a 2 2/12-year-old Japanese patient who was born with a normal birth size (length, +0.2 SD; weight, −0.5 SD) and showed postnatal growth failure (height, −3.1 SD; weight, −3.4 SD), hypotonia, frontal bossing, micrognathia, and small hands. Methylation analysis, genotyping analysis, and deletion analysis were performed with blood samples of the patient and the parents, showing that the DMRs of this patient were grossly hypomethylated in the absence of upd(14)mat and deletion of the DMRs. The results indicate the occurrence of an epimutation (hypomethylation) affecting the normally methylated DMRs of paternal origin, and imply that epimutations should be examined in patients with upd(14)mat-like phenotype.
European Journal of Human Genetics (2008) **16**, 1019–1023; doi:10.1038/ejhg.2008.90; published online 14 May 2008

Keywords: epimutation; growth failure; imprinting; differentially methylated region; upd(14)mat

Introduction

Maternal uniparental disomy for chromosome 14 (upd(14)mat) results in clinically discernible features such as pre- and postnatal growth failure, hypotonia, obesity, small hands, and early onset of puberty.[1] Phenotypic development is consistent with chromosome 14q32.2 region harboring several paternally expressed genes (*PEGs*) such as *DLK1* and *RTL1* and maternally expressed genes (*MEGs*) such as *MEG3* (alias *GTL2*), *RTL1as* (*RTL1* antisense), and *MEG8*.[2,3] The parent-of-origin-specific monoallelic expression patterns are tightly related to methylation status of differential methylation regions (DMRs).[4] For the 14q32.2 imprinted region, the previous studies have identified the intergenic DMR (IG-DMR) between *DLK1* and *MEG3* and the *MEG3*-DMR that are severely hypermethylated after paternal transmission and grossly hypomethylated after maternal transmission.[5–7] In particular, the germline-derived IG-DMR plays a pivotal role in the imprinting regulation, because methylation pattern of the secondary *MEG3*-DMR is dependent on that of the IG-DMR.[8]

The upd(14)mat-like phenotype has also been exhibited by non-disomic patients. Temple *et al*[9] described a patient

*Correspondence: Dr T Ogata, Department of Endocrinology and Metabolism, National Research Institute for Child Health and Development, 2-10-1 Ohkura, Setagaya, Tokyo 157-8535, Japan.
Tel: +81 2 5494 7025; Fax: +81 2 5494 7026;
E-mail: tomogata@nch.go.jp
Received 10 January 2008; revised 25 March 2008; accepted 3 April 2008; published online 14 May 2008

with upd(14)mat-like phenotype and an epimutation (hypomethylation) of the normally methylated DMR of paternal origin. Kagami *et al*[5] reported three patients with upd(14)mat-like phenotype and microdeletions affecting the 14q32.2 imprinted region including the DMRs of paternal origin. In this regard, the IG-DMR deletion from the paternally derived chromosome has no effect on the imprinting status, although that from the maternally derived chromosome results in a maternal to paternal epigenotypic alteration.[5,7] Thus, simple genotype–phenotype correlations can be applied for the three patients with the microdeletions, implying that loss of paternally derived *DLK1* and *RTL1* constitutes primary additive underlying factors for the development of upd(14)mat-like phenotype, although the perturbation of other imprinted genes could also have some effects.[5]

Here, we report an epimutation identified in a patient with upd(14)mat-like phenotype.

Patient and methods

Case report

This Japanese girl was born at 41 weeks of gestation after natural conception, with a history of mild oligohydramnios in the third trimester. At birth, her length was 50.0 cm (+0.2 SD), her weight 3.03 kg (−0.5 SD), and her head circumference 34.5 cm (+0.8 SD). The non-consanguineous parents were clinically normal, and the height was 161.0 cm (−1.7 SD) for the father and 154.5 cm (−0.7 SD) for the mother.

At 5 months of age, she was referred to us, because she was unable to control her head. Physical examination revealed generalized hypotonia without palsy and abnormal tendon reflex, and several somatic features such as frontal bossing, micrognathia, and small hands (Supplementary Figure 1). In addition, her length became below −2 SD of the mean from 10 months of age, while hypotonia was gradually ameliorated. She controlled her head at 7 months of age, sat without support at 11 month, and walked without support at 19 months. Repeatedly performed biochemical studies for hypotonia and growth failure were normal, as were skeletal roentgenograms and brain magnetic resonance imaging. The karyotype was 46XX in all the 30 lymphocytes examined. With a provisional diagnosis of Prader–Willi syndrome (PWS) that is primarily based on hypotonia and growth deficiency, fluorescence *in situ* hybridization (FISH) analysis for *SNRPN* and methylation analysis for the DMR at the *SNRPN* promoter region were performed,[10] showing normal findings. In addition, hypomethylation of the *H19*-DMR and upd(7)mat, which can cause growth failure, were also excluded by previous methods.[11,12] On the last examination at 2 2/12 years of age, her height was 76.1 cm (−3.1 SD), her weight 7.9 kg (−3.4 SD), and her head circumference 44.9 cm (−1.9 SD). Her mental development appeared age appropriate.

Methylation analysis

This study was approved by the Institutional Review Board Committees at Hokkaido University Hospital and National Center for Child Health and Development. After obtaining written informed consent, we examined the IG-DMR (CG4 and CG6) and the *MEG3*-DMR (Figure 1a), using bisulfite-treated leukocyte genomic DNA. For the IG-DMR, bisulfite sequencing was performed as reported previously,[5] and the SNPs (*rs12437020* for CG4 and *rs10133627* for CG6) were also genotyped. For the *MEG3*-DMR, PCR amplification was performed with methylated and unmethylated allele-specific primers, as described previously.[5,6] A hitherto unreported upd(14)mat patient and the previously reported upd(14)pat patient[5] were similarly analyzed with permission.

Genotyping analysis

We performed microsatellite analysis for 16 loci on chromosome 14 and SNP analysis for 39 loci around the DMRs (Supplementary Table 1). The primers used were as reported previously.[5]

Deletion analysis

Lymphocyte metaphase spreads were hybridized with a long and accurate (LA)-PCR product encompassing the IG-DMR and that spanning the *MEG3*-DMR (Figure 1a), together with an RP11-566I2 probe for 14q12 used as an internal control. Furthermore, the two LA-PCR products were also obtained from the patient and a control subject, and subjected to fragment size comparisons after restriction enzyme digestions, to detect a possible tiny deletion in the patient. The detailed methods for the deletion analysis have been reported previously.[5]

Results

Methylation analysis

The results are shown in Figure 1b. For the IG-DMR, CG4 and CG6 were grossly hypomethylated in the patient and the upd(14)mat patient, severely methylated in the upd(14)pat patient, and delineated in apparently mosaic patterns in the parents. In addition, the CG4 SNP typing indicated parental origin-dependent methylation patterns in the parents, and heterodisomy for the this region in the upd(14)mat patient. The CG6 SNP typing data were not informative. For the *MEG3*-DMR, PCR products were obtained with an unmethylated allele-specific primer pair alone in the patient and the upd(14)mat patient, with a methylated allele-specific primer pair alone in the upd(14)pat patient, and with both primer pairs in the parents.

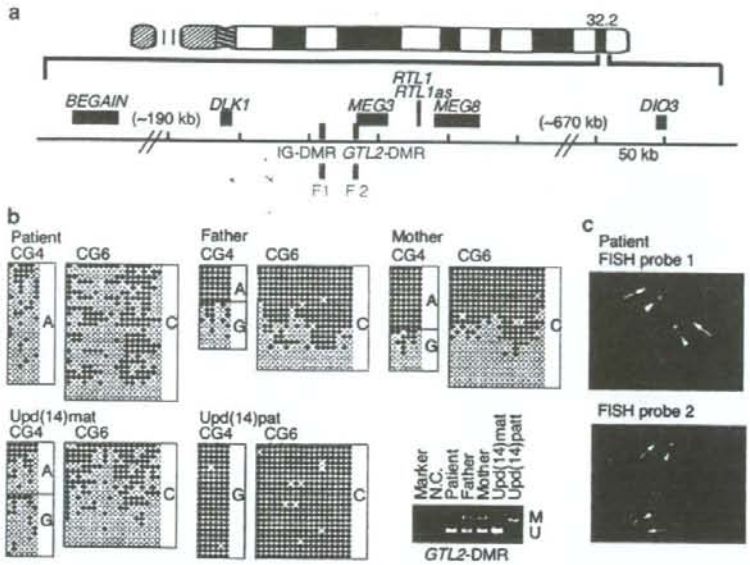

Figure 1 Summary of the molecular studies. (**a**) The regional physical map of the human chromosome 14q32.2 imprinted region. *PEGs* are shown in blue and *MEGs* in red; although it remains to be clarified whether *DIO3* is a *PEG*, mouse *Dio3* is known to be preferentially but not exclusively expressed from a paternally derived chromosome in embryos.[13] *WDR25* and *BEGAIN* appear biparentally expressed genes. The IG-DMR and the *MEG3*-DMR are depicted in green, and the FISH probes 1 and 2 covering the DMRs indicated in orange. The physical distance is ~190 kb between *BEGAIN* and *DLK1*, ~170 kb between *DLK1* and *MEG8*, and ~670 kb between *MEG8* and *DIO3*. (**b**) Methylation patterns of the IG-DMR (CG4 and CG6) and the *MEG3*-DMR. Bisulfite sequencing has been performed for CG4 and CG6. Each line indicates a single clone and each circle denotes a CpG island; filled and open circles represent methylated and unmethylated cytosines, respectively. The SNP typing data for CG4 and CG6 are also shown. Methylated (M) and unmethylated (U) allele-specific PCR amplification has been performed for the *MEG3*-DMR. NC: negative control. (**c**) FISH analysis using FISH probe 1 (F1) for the IG-DMR and FISH probe 2 (F2) for the *MEG3*-DMR. The red signals (arrows) have been detected by the two FISH probes and the green signals (arrowheads) have been identified by an RP11-566I2 probe for 14q12 used as an internal control.

Genotyping analysis

Microsatellite analysis demonstrated biparental origin of the two chromosome 14 homologs, and SNP analysis ndicated lack of a segmental upd(14)mat around the DMRs (Supplementary Table 1).

Deletion analysis

FISH probes 1 and 2 detected two signals in the patient (Figure 1c). The fragment size comparison after enzyme digestions showed no abnormal bands suggestive of a tiny deletion in the patient.

Discussion

This patient had hypomethylated DMRs in the absence of discernible maternal disomy affecting the DMRs or loss of the paternally derived DMRs. This implies the occurrence of an epimutation (hypomethylation) affecting the normally methylated DMRs of paternal origin. To our knowledge, such an epimutation (hypomethylation) has previously been identified only in a patient reported by Temple *et al*.[9] Actually, the DMR examined in that patient appears to be a part of the *MEG3*-DMR rather than the IG-DMR on the basis of its position. It is likely, however, that the IG-DMR is also hypomethylated in that patient, because the *MEG3*-DMR can stay hypomethylated only in the presence of the hypomethylated IG-DMR.[8]

Clinical features of the two patients with epimutation are summarized in Table 1, together with those of upd(14)mat patients. Notably, clinical features are grossly similar in epimutation patients and upd(14)mat patients. Although our patient had no prenatal growth failure, lack of prenatal and/or postnatal growth failure has been described in several upd(14)mat patients,[14–16] and this would be due to body growth being a multifactorial trait subject to multiple genetic and environmental factors.[17] In this regard, it has been reported that clinical features are comparable between patients with paternal upd(14) and those with epimutations (hypermethylation) affecting the normally hypomethylated DMRs of maternal origin.[5] Taken together, the methylation patterns of the DMRs appear to be closely related to the expression patterns of virtually all the imprinted genes on 14q32.2.

It is noteworthy that the patient was initially suspected as having PWS. Indeed, growth deficiency, hypotonia, and small hands are shared by upd(14)mat and PWS,[18,19] and

Table 1 Clinical phenotypes in patients with epimutations and upd(14)mat

	Epimutations		*Upd(14)mat*
	This report	*Temple* et al[9]	*(n = 35)*[a]
Age	2 2–12 years	10 7–12 years	0–30 years
Sex	Female	Male	M:F = 17:18
Premature delivery	–	–	10/25
Prenatal growth failure	–	+	24/27
Postnatal growth failure	+	+	26/32
Somatic features	+	+	23/35[b]
Frontal bossing	+	+	9/9
High arched palate	–	+	7/9
Micrognathia	+	–	5/5
Small hands	+	+	24/27
Scoliosis	–	+	5/19
Others			
Hypotonia	+	+	25/28
Obesity	–	–	14/34
Early onset of puberty	Unknown	Borderline	14/16
Mental retardation	–	–	10/27
Thyroid dysfunction	–	–	ND

ND: not described.
In the column summarizing the clinical features of 35 patients with upd(14)mat, the denominators indicate the number of patients examined for the presence or absence of each feature, and the numerators represent the number of patients assessed to be positive for that feature; thus, the differences between the denominators and the numerators denote the number of patients evaluated to be negative for that feature.
[a]Patients with maternal uniparental disomy for chromosome 14 reported in the literature, several upd(14)mat patients with no phenotypic description have not been included. The references for the 35 upd(14)mat patients are summarized in Kagami *et al*.[5]
[b]The ratio of patients with at least one somatic feature.

upd(14)mat has occasionally been identified in patients referred for molecular examination of PWS.[19,20] Thus, upd(14)mat and epimutations should be considered in patients with PWS-like phenotype.[18,19]

In summary, we observed an epimutation (hypomethylation) of the paternally derived DMRs in a patient with upd(14)mat-like phenotype. Further studies will identify epimutations in patients with upd(14)mat-like phenotype, thereby contributing to clarify the relevance of epimutations in human imprinted disorders.

Acknowledgements

This study was supported by grants for Child Health and Development (20C-2) and for Research on Children and Families (H18-005) from the Ministry of Health, Labor, and Welfare, and by Grants-in-Aid for Scientific Research (Priority Areas: 16086215) from the Ministry of Education, Culture, Sports, Science and Technology.

Disclosure

The authors have reported no conflicts of interest.

References

1 Kotzot D: Maternal uniparental disomy 14 dissection of the phenotype with respect to rare autosomal recessively inherited traits, trisomy mosaicism, and genomic imprinting. *Ann Genet* 2004; 47: 251–260.
2 Cavaille J, Seitz H, Paulsen M, Ferguson-Smith AC, Bachellerie JP: Identification of tandemly-repeated C/D snoRNA genes at the imprinted human 14q32 domain reminiscent of those at the Prader-Willi/Angelman syndrome region. *Hum Mol Genet* 2002; 11: 1527–1538.
3 Charlier C, Segers K, Wagenaar D *et al*: Human-ovine comparative sequencing of a 250-kb imprinted domain encompassing the callipyge (clpg) locus and identification of six imprinted transcripts: DLK1, DAT, GTL2, PEG11, antiPEG11, and MEG8. *Genome Res* 2001; 11: 850–862.
4 Li E, Beard C, Jaenisch R: Role for DNA methylation in genomic imprinting. *Nature* 1993; 366: 362–365.
5 Kagami M, Sekita Y, Nishimura G *et al*: Deletions and epimutations affecting the human chromosome 14q32.2 imprinted region: implications for the phenotypic development in paternal and maternal uniparental disomy for chromosome 14. *Nat Genet* 2008; 40: 237–242.
6 Murphy SK, Wylie AA, Coveler KJ *et al*: Epigenetic detection of human chromosome 14 uniparental disomy. *Hum Mutat* 2003; 22: 92–97.
7 Lin SP, Youngson N, Takada S *et al*: Asymmetric regulation of imprinting on the maternal and paternal chromosomes at the Dlk1-Gtl2 imprinted cluster on mouse chromosome 12. *Nat Genet* 2003; 35: 97–102.
8 Takada S, Paulsen M, Tevendale M *et al*: Epigenetic analysis of the Dlk1-Gtl2 imprinted domain on mouse chromosome 12: implications for imprinting control from comparison with Igf2-H19. *Hum Mol Genet* 2002; 11: 77–86.
9 Temple IK, Shrubb V, Lever M, Bullman H, Mackay DJ: Isolated imprinting mutation of the DLK1/GTL2 locus associated with a clinical presentation of maternal uniparental disomy of chromosome 14. *J Med Genet* 2007; 44: 637–640.
10 The ASHG/ACMG Test and Technology Transfer Committee: Diagnostic testing for Prader–Willi and Angelman syndromes. *Am J Hum Genet* 1996; 58: 1085–1088.

11 Kagami M, Nagai T, Fukami M, Yamazawa K, Ogata T: Silver-Russell syndrome in a girl born after *in vitro* fertilization: partial hypermethylation at the differentially methylated region of PEG1/MEST. *J Assist Reprod Genet* 2007; **24**: 131–136.
12 Yamazawa K, Kagami M, Ogawa M, Horikawa R, Ogata T: Placental hypoplasia in maternal uniparental disomy for chromosome 7. *Am J Med Genet A* 2008; **146**: 514–516.
13 Tsai CE, Lin SP, Ito M, Takagi N, Takada S, Ferguson-Smith AC: Genomic imprinting contributes to thyroid hormone metabolism in the mouse embryo. *Curr Biol* 2002; 12: 1221–1226.
14 Rosa AL, Wu YQ, Kwabi-Addo B, Coveler KJ, Reid Sutton V, Shaffer LG: Allele-specific methylation of a functional CTCF binding site upstream of MEG3 in the human imprinted domain of 14q32. *Chromosome Res* 2005; 13: 809–818.
15 Aretz S, Raff R, Woelfle J *et al*: Maternal uniparental disomy 14 in a 15-year-old boy with normal karyotype and no evidence of precocious puberty. *Am J Med Genet A* 2005; 135: 336–338.
16 Takahashi I, Takahashi T, Utsunomiya M, Takada G, Koizumi A: Long-acting gonadotropin-releasing hormone analogue treatment for central precocious puberty in maternal uniparental disomy chromosome 14. *Tohoku J Exp Med* 2005; 207: 333–338.
17 Vogel F, Motulsky AG: *Human Genetics: Problems and Approaches*. Heidelberg: Springer-Verlag, 1986.
18 Gunay-Aygun M, Schwartz S, Heeger S, O'Riordan MA, Cassidy SB: The changing purpose of Prader–Willi syndrome clinical diagnostic criteria and proposed revised criteria. *Pediatrics* 2001; 108: E92.
19 Berends MJ, Hordijk R, Scheffer H, Oosterwijk JC, Halley DJ, Sorgedrager N: Two cases of maternal uniparental disomy 14 with a phenotype overlapping with the Prader–Willi phenotype. *Am J Med Genet* 1999; **84**: 76–79.
20 Mitter D, Buiting K, von Eggeling F *et al*: Is there a higher incidence of maternal uniparental disomy 14 [upd(14)mat]? Detection of 10 new patients by methylation-specific PCR. *Am J Med Genet A* 2006; **140**: 2039–2049.

Supplementary Information accompanies the paper on European Journal of Human Genetics website (http://www.nature.com/ejhg)

J Mol Med (2008) 86:1171–1181
DOI 10.1007/s00109-008-0377-4

ORIGINAL ARTICLE

Molecular and clinical findings and their correlations in Silver-Russell syndrome: implications for a positive role of IGF2 in growth determination and differential imprinting regulation of the *IGF2–H19* domain in bodies and placentas

Kazuki Yamazawa · Masayo Kagami · Toshiro Nagai · Tatsuro Kondoh · Kazumichi Onigata · Katsuhiro Maeyama · Tomonobu Hasegawa · Yukihiro Hasegawa · Toshio Yamazaki · Seiji Mizuno · Yoko Miyoshi · Shinichiro Miyagawa · Reiko Horikawa · Kentaro Matsuoka · Tsutomu Ogata

Received: 18 March 2008 / Revised: 8 May 2008 / Accepted: 30 May 2008 / Published online: 8 July 2008
© Springer-Verlag 2008

Abstract Silver-Russell syndrome (SRS) is characterized by growth failure and dysmorphic features and is frequently caused by hypomethylation (epimutation) of the *H19*-DMR. Although molecular and clinical studies have extensively been performed for SRS patients themselves, such studies have not been carried out for placentas. We identified 20 epimutation-positive and 40 epimutation-negative Japanese SRS patients and obtained placental weight data from 12 epimutation-positive and ten epimutation-negative patients and paraffin-embedded placental tissues for molecular and histological examinations from three epimutation-positive and two epimutation-negative patients. Methylation patterns

Electronic supplementary material The online version of this article (doi:10.1007/s00109-008-0377-4) contains supplementary material, which is available to authorized users.

K. Yamazawa · M. Kagami · T. Ogata (✉)
Department of Endocrinology and Metabolism,
National Research Institute for Child Health and Development,
Tokyo, Japan
e-mail: tomogata@nch.go.jp

K. Yamazawa · T. Hasegawa
Department of Pediatrics, Keio University School of Medicine,
Tokyo, Japan

T. Nagai
Department of Pediatrics,
Dokkyo Medical University Koshigaya Hospital,
Koshigaya, Japan

T. Kondoh
Department of Pediatrics,
Nagasaki University Graduate School of Biomedical Sciences,
Nagasaki, Japan

K. Onigata
Department of Pediatrics and Developmental Medicine,
Gunma University Graduate School of Medicine,
Maebashi, Japan

K. Maeyama
Department of Pediatrics, Saitama City Hospital,
Saitama, Japan

Y. Hasegawa
Endocrinology and Metabolism Unit,
Tokyo Metropolitan Kiyose Children's Hospital,
Kiyose, Japan

T. Yamazaki
Department of Pediatrics, School of Medicine,
Fujita Health University,
Toyoake, Japan

S. Mizuno
Department of Pediatrics, Central Hospital,
Aichi Human Service Center,
Kasugai, Japan

Y. Miyoshi
Department of Pediatrics,
Osaka University Graduate School of Medicine,
Suita, Japan

were comparable between leukocytes and placentas in both epimutation-positive and epimutation-negative patients. Epimutations resulted in virtually no *IGF2* expression and biallelic slight *H19* expression in the leukocytes and obviously reduced *IGF2* expression of paternal origin and nearly normal *H19* expression of maternal origin in the placentas. Epimutation-positive patients had characteristic body phenotype and small placentas with hypoplastic chorionic villi, and epimutation-negative patients had somewhat small placentas with hypoplastic chorionic villi or massive infarction. Furthermore, significant correlations were identified between the *H19*-DMR methylation index and the body and placental sizes and between the placental weight and the body size in the epimutation-positive patients, whereas such correlations were not detected for the head circumference. These results suggest (1) characteristic phenotype and reduced *IGF2* expression in the epimutation-positive placentas; (2) similarities and differences in the epigenetic control of the *IGF2–H19* domain between leukocytes and placentas; (3) a positive role of the *IGF2* expression level, as reflected by the methylation index, in the determination of body and placental growth in epimutation-positive patients, except for the brain where *IGF2* is expressed biallelically; (4) involvement of placental dysfunction in prenatal growth failure; and (5) relevance of both (epi)genetic factor(s) and environmental factor(s) to SRS in epimutation-negative patients.

Keywords Silver-Russell syndrome · *H19*-DMR · Epimutation · IGF2 · Placenta · Correlation

Introduction

Silver-Russell syndrome (SRS) is a congenital developmental disorder characterized by pre- and postnatal growth failure, relative macrocephaly, triangular face, hemihypotrophy, and fifth-finger clinodactyly [1]. Recent studies have shown that hypomethylation (epimutation) of the paternally derived differentially methylated region in the upstream of *H19* (*H19*-DMR, also known as the imprinting control region 1 on chromosome 11p15.5) accounts for 30–65% of SRS patients [2–6]. In this regard, it is known that a common enhancer is shared by the paternally expressed gene *IGF2* (insulin-like growth factor 2) and the maternally expressed gene *H19* [7] and that the enhancer exerts its effects on *IGF2* or *H19* depending on the methylation status of the *H19*-DMR [8, 9]. This alternative enhancer effect is mediated by an insulator protein CTCF that binds to the unmethylated *H19*-DMR of maternal origin but not to the methylated *H19*-DMR of paternal origin [10, 11]. Thus, it has been postulated that the hypomethylation of the paternally derived *H19*-DMR results in maternalization of the *IGF2–H19* imprinted domain, leading to the development of SRS because of reduced *IGF2* expression [2], although the exaggerated *H19* expression might also exert some effect. Indeed, reduced *IGF2* expression has been shown in cultured skin fibroblasts from two SRS patients [2], while the postnatal serum IGF2 level was not decreased [5, 12]. These findings, together with the identification of maternal uniparental disomy for chromosome 7 (upd(7)mat) in 7–10% of SRS patients [1] imply that SRS primarily represents an epigenetic disorder. In this regard, hypermethylation of the KvDMR1 (also known as the imprinting control region 2 on 11p15.5) just centromeric to the *H19*-DMR might also lead to SRS via some mechanism (s) such as overexpression of a negative growth regulator *CDKN1C* [13], although such hypermethylation has not been reported to date.

Virtually all the imprinted genes studied to date are expressed in the placenta [14]. This is consistent with the notion that imprinted genes are identified from placental mammals and play a pivotal role in placental growth and development [14, 15]. Indeed, placental hypoplasia has been identified in SRS patients with upd(7)mat [16], and placentomegaly has been described in Beckwith-Wiedemann syndrome patients with upd(11)pat involving the *IGF2–H19* imprinted domain [17] and in patients with upd(14)pat [18]. These findings, together with the results of knockout mouse experiments for imprinted genes [19] and the human growth data in various uniparental disomies [20, 21], imply that placental growth as well as fetal growth is promoted by paternally expressed genes and suppressed by maternally expressed genes. Furthermore, recent studies have revealed that methylation profiles of the germline derived DMRs are similar, but those of secondary DMRs are different between the body and the placenta and that some mechanism(s) other than parental origin-specific methylation patterns also plays a certain role in placental imprinting regulation [15, 18, 22, 23].

To our knowledge, however, although extensive studies have been performed for SRS patients, there has been no report describing molecular and clinical findings of pla-

S. Miyagawa
Department of Pediatrics,
National Hospital Organization Kure Medical Center,
Kure, Japan

R. Horikawa
Division of Endocrinology and Metabolism,
National Center for Child Health and Development,
Tokyo, Japan

K. Matsuoka
Division of Pathology,
National Center for Child Health and Development,
Tokyo, Japan